ELSEVIER

Journal of Alloys and Compounds 325 (2001) 223–229

Journal of ALLOYS AND COMPOUNDS

www.elsevier.com/locate/jallcom

Preparation and characterization of sol–gel-derived unsupported Al_2O_3–SiO_2 composite membranes

Qi Wei[a,*], Dawei Wang[b], Shugen Zhang[b], Chusheng Chen[a]

[a]*Department of Materials Science and Engineering, University of Science and Technology of China, Hefei, Anhui 230026, PR China*
[b]*College of Resources, Environment and Civil Engineering, Central South University of Technology, Changsha, Hunan 410083, PR China*

Received 4 January 2001; accepted 13 March 2001

Abstract

The synthesis of unsupported Al_2O_3–SiO_2 composite membranes has been achieved by controlling hydrolysis and condensation of aluminium iso-propoxide and tetraethyl silicate under acidic conditions. The phase transformation and pore structural evolution of composite membranes are investigated by X-ray diffraction and nitrogen adsorption measurement, respectively. After sintering at 600°C for 10 h, the composite membranes consist of only amorphous phase as SiO_2 concentration ranges from 25 to 100 mol% and crystalline γ-Al_2O_3 appears at lower SiO_2 content. Both micropores and mesopores contribute to the total pore volume and BET surface area, and mesopores become dominant. At high SiO_2 content (50 mol%), the composite materials exhibit a 1-nm pore diameter decrease and about 100 $m^2\ g^{-1}$ surface area increase, as well as only a negligible pore volume drop of 0.0164 $cm^3\ g^{-1}$, compared with the single Al_2O_3 membrane. For the composite membrane with 40 mol% SiO_2 concentration, sintering at higher temperature leads to phase transformation and grain growth, and both densification and phase transformation result in a decrease in both total pore volume and surface area, as well as an increase in mean pore diameter and finally the collapse of pores. Further study is required to improve the thermal stability of the composite membrane.

Keywords: Oxide materials; Composite materials; Sintering; Microstructure

1. Introduction

Inorganic ceramic membranes with their unique thermal, chemical and mechanical stability have received increased attention due to the promising application in gas separation, liquid separation and catalytic membrane reactors at high temperature and in chemically reactive environments [1–9]. Most previous studies have focused on the single oxide membranes such as Al_2O_3 [10–12], ZrO_2 [13,14], SiO_2 [15,16], TiO_2 [17,18] and so on, some of which have been commercially produced, but so far few studies on their binary and ternary composite membranes have been reported. Binary composite membranes may exhibit different pore structures and separation performances in comparison with the single oxide membranes because of the different chemical compositions and preparation conditions. For example, Al_2O_3–SiO_2 membranes could have the desired combination of the features of both the Al_2O_3 and SiO_2 components. The Al_2O_3 moiety usually offers good mechanical stability as well as catalytic properties. The SiO_2 species would provide the membranes with comparatively large surface area. That is the reason why modification of mesoporous alumina has attracted a great deal of attention in recent years.

Several approaches including the sol–gel route and the chemical vapor deposition (CVD) method have been developed for the modification of mesoporous alumina membranes [19–24]. The sol–gel process is to coat a microporous silica layer about several microns in thickness on the surface of the alumina membrane, so there exists an interface between the alumina membrane and its top microporous silica layer and the membranes behave separately during the separation process. We report here another sol–gel modification procedure. The method involves the separate preparation of silica sol and boehmite (AlOOH) sol by controlling hydrolysis and condensation of an inorganic precursor such as tetraethyl silicate (TEOS) and aluminium iso-propoxide, respectively. The SiO_2 sol was used to modify the AlOOH sol and their mixtures were allowed to gelate to form multiphase composite membranes. The present paper is intended to study the effects

*Corresponding author.
E-mail address: weiqi@ustc.edu.cn (Q. Wei).

0925-8388/01/$ – see front matter
PII: S0925-8388(01)01354-8

of chemical composition and heat treatment on the phase composition and pore structures for the Al_2O_3–SiO_2 composite membranes.

2. Experimental

2.1. Sample preparation

Boehmite sol and silica sol were prepared by controlling hydrolysis and condensation of aluminium iso-propoxide (Shanghai Reagent Co., China) and tetraethyl silicate (Shanghai Reagent Co., China) under acidic conditions using HNO_3 as catalyst, respectively, following similar procedures as reported previously [25,26]. The AlOOH and SiO_2 contents were calculated from the resultant stoichiometry assuming complete hydrolysis of both silicon and aluminium precursors. The freshly prepared boehmite sol and silica sol were mixed together at different molar ratios and then stirred for 1 h at room temperature. After aging for 24 h, the stable composite sols were allowed to gelate in the Petri dishes under ambient conditions. The gels were heated from room temperature at a rate of 0.5°C min^{-1} and sintered under atmosphere conditions at different temperatures (200–1100°C) for 10 h to get the cracks and Pinholes-free materials. Composite membranes with different chemical composition (molar content of SiO_2 component equals to 20, 25, 33, 40, and 50%, respectively) were designed to study the effects of chemical compositions on membrane pore structures. Single Al_2O_3 and SiO_2 membranes were also prepared for comparison.

2.2. Membrane characterization

The phase composition of the calcinated membranes was investigated by X-ray diffraction (XRD, D/MaxrA, Japan) at the operating condition of 30 kV–100 mA, using Cu Kα radiation. The porous structures were determined by nitrogen adsorption (Autosorb-1, Quantachrome Co., USA) measured at −196°C and relative pressure interval between 0.0125 and 0.998. Before each measurement, the samples were degassed at 200°C under vacuum for sufficient time ($5<t<10$ h) to observe the absence of significant changes in vacuum stability. The specific surface area was obtained from the BET equation, and pore size distribution was calculated from the desorption branch of the isotherms by the BJH method using the capillary condensation model assuming cylindrical pores.

3. Results and discussion

3.1. XRD study of the composite membranes

The X-ray diffraction patterns of composite membranes with different chemical compositions are shown in Fig. 1

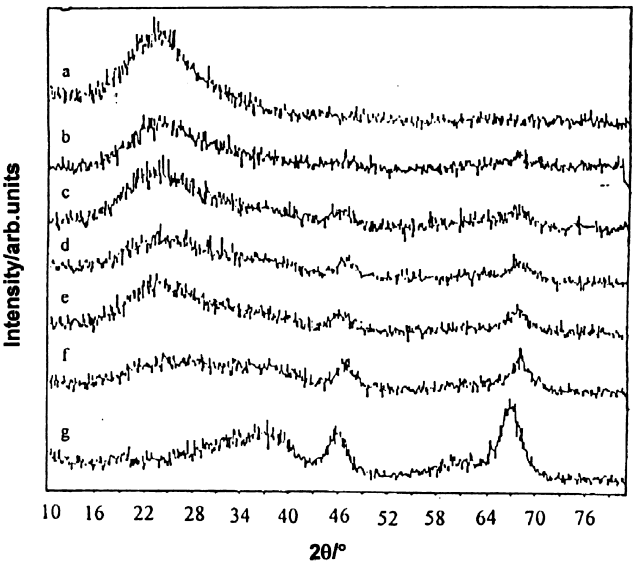

Fig. 1. XRD patterns for composite membranes with mol% of SiO_2 content: (a) 100%; (b) 50%; (c) 40%; (d) 33%; (e) 25%; (f) 20% and (g) 0% sintering at 600°C for 10 h.

for sintering for 10 h at 600°C. Only a dispersive peak at $2\theta=24°$ is observed in the single SiO_2 sample and obviously the peak is assigned to the non-crystalline SiO_2 (Fig. 1a). For the samples with 25–40 mol% SiO_2 component, two peaks at $2\theta=46$ and 68°, respectively are detected (Fig. 1b–e). The samples can also be identified as amorphous because the two peaks are too weak despite where γ-Al_2O_3 peaks usually appear according to Refs. [27,28]. The intensity of these two peaks becomes strong enough to be assigned as γ-Al_2O_3 as the SiO_2 content decreases to 20% and less (Fig. 1f,g). The broad 2θ interval of the γ-Al_2O_3 peaks reveals that the crystallite grains may be in the scale of nanometers. Since no peaks of binary oxides are identified in the XRD spectra, it is reasonable to conclude that the composite membranes are made of noncrystalline material when the SiO_2 content ranges from 25 to 100 mol%, and of amorphous and nanometer crystalline γ-Al_2O_3 when the SiO_2 content is less than 25 mol%.

Fig. 2 shows XRD patterns for the composite membranes with 40 mol% SiO_2 sintering from 200 to 1100°C for 10 h. From 200 to 800°C, the samples exist primarily as noncrystalline. When the temperature rises to 1000°C, two peaks identified as γ-Al_2O_3 appear at $2\theta=46$ and 68°, respectively. Phase transformation from γ- to α-Al_2O_3 and the formation of mullite phase occur when heating at 1100°C. The transformation temperature of γ- to α-Al_2O_3 phase in the present study is 100°C lower than that reported by Yeung [27]. The mechanism for this discrepancy is still not clear and requires further study. Heating at 1100°C brings about many changes in the samples. On the one hand, porosity will decrease because of densification caused by viscous sintering of amorphous particles by viscous flow during which the particle centres

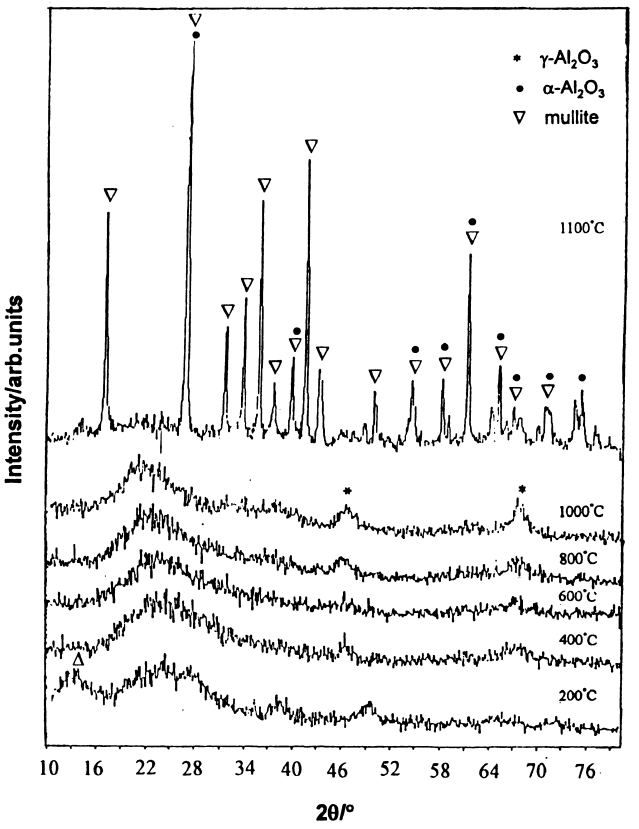

Fig. 2. XRD patterns for the composite membranes with 40 mol% SiO_2 content sintering at different temperatures from 200 to 1100°C, respectively for 10 h.

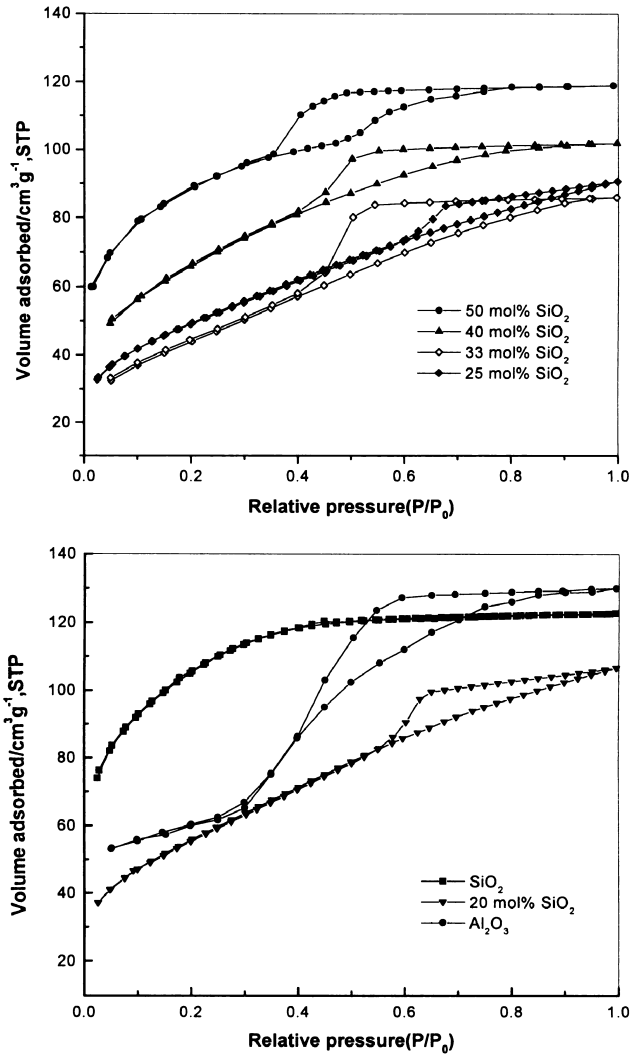

Fig. 3. N_2 adsorption–desorption isotherms at −196°C for the alumina and silica as well as composite membranes sintering at 600°C for 10 h.

approach each other. The average interparticle pore size will first grow due to the 'consumption' of smaller particles by larger ones [29] and then dramatically drops because the pores are expelled to the surface of samples as the sintering goes on. On the other hand, a considerable growth of the crystallites grains from the range of nanometers (when sintering at 1000°C) to microns is accompanied by an increase in the sintering activity. The phase transformation and crystallite growth should usually be avoided because they cause the same pore structure evolution as induced by the densification process. This change of pore structure will be proved in the next section.

3.2. Influence of chemical composition on porous structure of composite membranes

The nitrogen adsorption–desorption isotherms for the composite membranes with different molar percentages of SiO_2, as well as those of single alumina and silica membranes, are shown in Fig. 3. The isotherm of the single alumina membrane can be classified as type IV in accordance with the BDDT classification. The presence of hysteresis loop classified as type H2 according to the IUPAC classification confirms that capillary condensation takes place and mesopores predominate in the membrane. The SiO_2 membrane, however, exhibits a typical isotherm of type I which is significantly different from that of the alumina membrane. The nitrogen adsorbed plateau at the relative pressure above 0.5 reveals that the membrane mainly contains micropores. The isotherms of composite membranes are similar to that of Al_2O_3 membrane, but the hysteresis loops deviate slightly from the type H2, thus suggesting that SiO_2 content could have brought some micropores into the composite membranes. The relative contribution of mesopores and micropores to the resultant pore volumes will be discussed below.

It is generally believed that the pore size distribution of membranes with Type IV-like isotherms can be measured by the BJH method based on the Kelvin equation. On the basis of thermodynamic considerations, the Kelvin equation is not valid for micropores and only valid for larger mesopores. Nevertheless the method has recently been applied to considerably lower pore diameter limits (1.3–1.7 nm) [30,31]. In order to examine the micropores possibly introduced by the silica content into the composite membranes, we extend the lower limit of pore diameter to

1.2 nm. Fig. 4 shows the pore size distribution of alumina membrane and the composite ones sintering at 600°C for 10 h. All the dominant pore radii are in the mesopore range with major peaks at 1.7–3.2 nm. The extension of the curves into submesopore range suggests the existence of micropores in the composite membranes, which is in good agreement with the results from the isotherm measurements. The pore radius shifts to a lower value and the distribution becomes sharper as the SiO_2 content increases. The sample with 50 mol% content shows a bimodal distribution with a second peak at 0.8 nm. The underlying mechanism for such a bimodal distribution can be contributed by the SiO_2 clusters which form a great deal of micropores in the membranes. Nevertheless the single Al_2O_3 membrane, with a total pore volume of 0.2 $cm^3\ g^{-1}$ and surface area of 206.5 $m^2\ g^{-1}$, contains no micropores. As discussed above, it is impossible to calculate the pore size distribution of the SiO_2 membrane by the BJH method (in fact, the quantitative determination of micropore size distribution is still an ambiguous problem and needs further study [30,31]), but the total pore volume and surface area can be obtained by the same method as applied in the composite membranes, amounting to 0.197 $cm^3\ g^{-1}$ and 381.6 $m^2\ g^{-1}$, respectively.

The total pore volume of composite membranes is illustrated in Fig. 5 as a function of SiO_2 content. With the increase in SiO_2 component, the total volume first drops to about 0.135 $cm^3\ g^{-1}$ and then increases in proportion to the SiO_2 content, reaching a maximum value of 0.186 $cm^3\ g^{-1}$ at the 50 mol% SiO_2 content. The fraction of micropore volume V_{Mic}% in the total pore volume is calculated by the following equation:

$$V_{Mic}\% = \frac{V_T - V_{Meso}}{V_T} \times 100\%$$

where V_T is the total pore volume and V_{Meso} is the mesopore volume which can be obtained by integrating the pore size distribution curves in Fig. 4 from 10 Å to infinity. As also demonstrated in Fig. 5, the percentage of micropore volume varies slightly at 20% when the SiO_2 content ranges from 20 to 40 mol% (except that of only 8% at the 33 mol% SiO_2 content), but rises abruptly to 34.7% at the 50 mol% SiO_2 content. One can also see from Fig. 6 that the mean pore radius decreases from 1.6 to 1.2 nm and the specific surface area increases from 197 to 306 $m^2\ g^{-1}$ as the SiO_2 content increases from 20 to 50 mol%. For the composite membrane with 50 mol% SiO_2 concentration, the modification of Al_2O_3 membranes with SiO_2 species leads to a 1-nm diameter decrease and about 100 $m^2\ g^{-1}$ surface area increase, as well as only a negligible reduction of 0.0164 $cm^3\ g^{-1}$ in pore volume compared with the single Al_2O_3 membrane. According to previous literature [32,33], the mesopore network in single

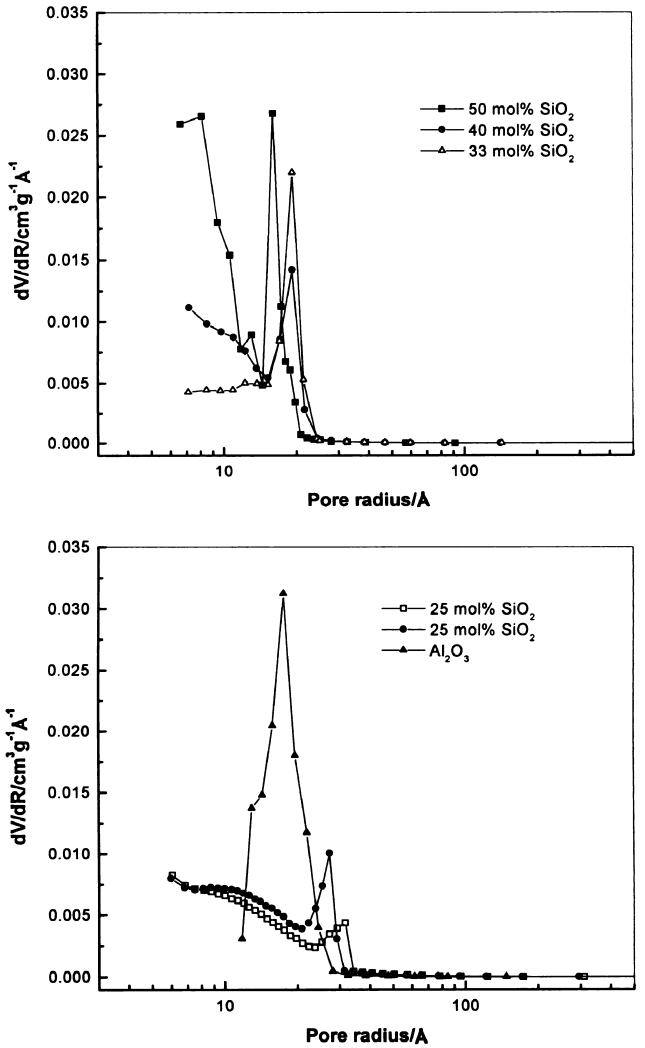

Fig. 4. BJH pore size distributions calculated from N_2 desorption isotherms for the alumina and composite membranes sintering at 600°C for 10 h.

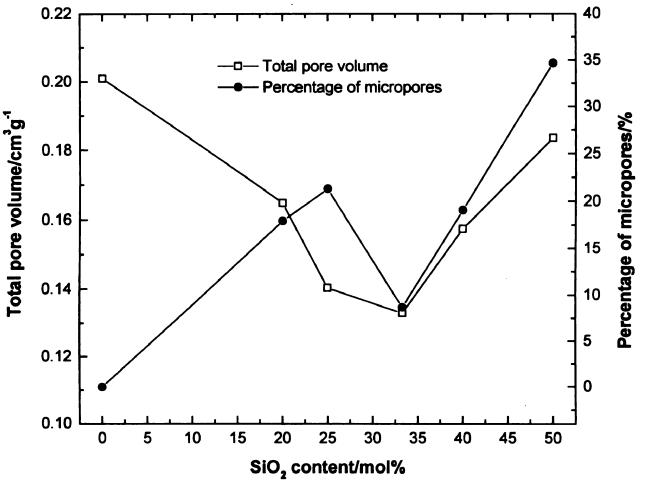

Fig. 5. SiO_2 content dependence of total pore volume and micropore percentage for the alumina and composite membranes sintering at 600°C for 10 h.

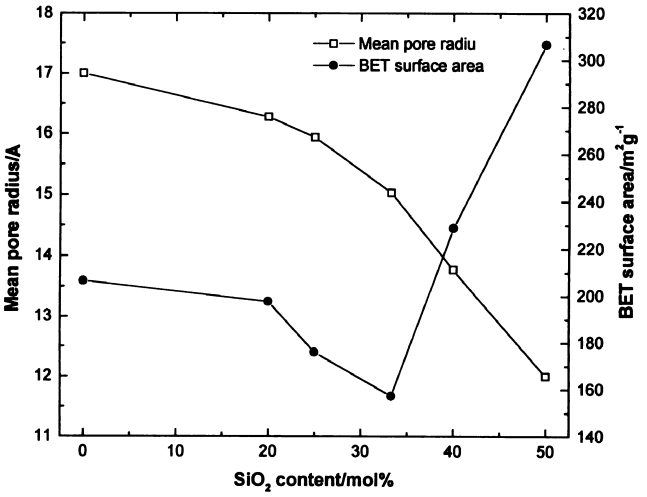

Fig. 6. SiO_2 content dependence of mean pore radius and BET surface area for the alumina and composite membranes sintering at 600°C for 10 h.

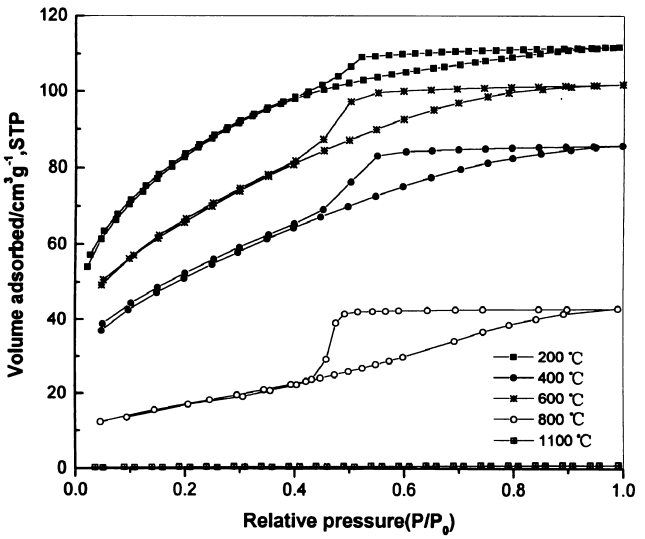

Fig. 7. N_2 adsorption–desorption isotherms at −196°C for composite membranes with 40 mol% SiO_2 content sintering at different temperature for 10 h.

alumina membrane is obtained by the packing of Al_2O_3 particles and micropores in silica membrane result from the aggregation and interpenetration of SiO_2 fractal clusters during gelation and membrane formation. It is easy to understand that the composite membranes possess porous structures of both Al_2O_3 and SiO_2 membranes because the evolution of their porous network is controlled by both particle packing and cluster aggregation mechanisms.

3.3. Influence of sintering on porous structure of the composite membrane

The isotherms of the composite membranes with 40 mol% SiO_2 content sintering from 200 to 1100°C for 10 h, respectively are shown in Fig. 7. For the five sintering membranes, the one at 200°C has a maximum saturated gas adsorption, and N_2 adsorption of the one at 1100°C is close to zero, indicating that there are no pores in this membrane and it is in good agreement with the assumption discussed in Section 3.1.

As shown in Fig. 8, the composite membranes sintering from 200 to 600°C have a wider pore size distribution than the one sintering at 800°C, the extension of the curves into the micropore scope illustrating the presence of micropores. The pore volume varying with sintering temperature is shown in Fig. 9, which shows a decrease for both the total pore volume and the micropore fraction except for sintering at 600°C. The BET surface area decreases and the mean pore radius increases after sintering (except at 600°C), as shown in Fig. 10. At 200°C, most water and ethanol in the gel are vaporized and leave behind an enormous amount of cavities which provide small pore radius, large surface area and high porosity in membranes. When the temperature rises to 400°C, the amorphous gels go through the so-called calcination step during which the organic additives continue to burn out and some gel clusters are transformed to dehydrated particles with some cavities beginning to unite, thus resulting in an increase in pore size and a decrease in pore volume (including micropore volume) and surface area. During heating at higher temperature (600°C), some pores become more compact and even divide into more pores when some shrinkage occurs, so there is a decrease in mean pore size and an increase in both pore volume and surface area. The increase in micropore percentage can be explained by the possibility that some mesopores have been compacted or divided into micropores. As the sintering temperature continues to rise (>800°C), the particles close up to each other and the mean pore size will grow at the cost of a

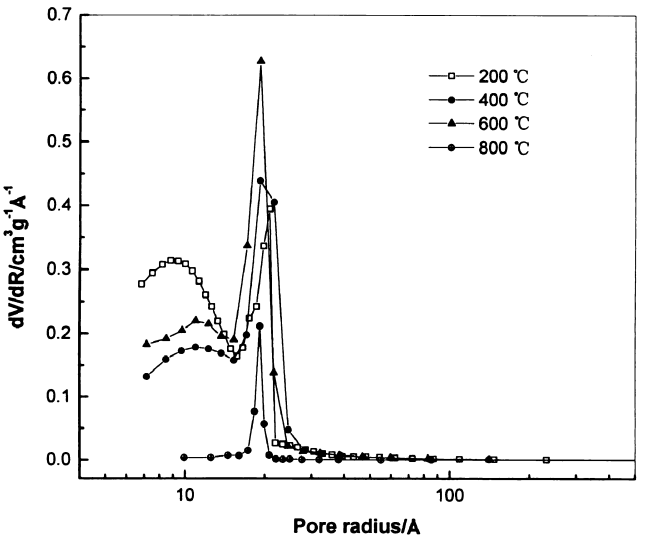

Fig. 8. BJH pores size distributions calculated from N_2 desorption isotherms for composite membranes with 40 mol% SiO_2 content sintering at different temperature for 10 h.

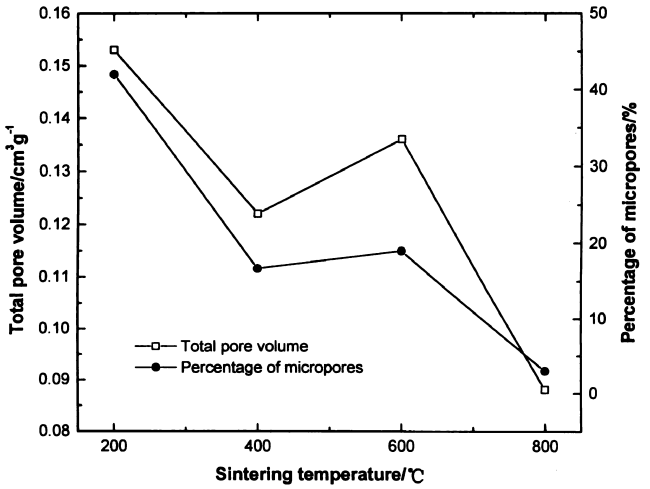

Fig. 9. Sintering temperature dependence of total pore volume and micropore percentage for composite membranes with 40 mol% SiO_2 content.

decrease in both surface area and porosity because small particles are 'swallowed up' by larger ones. In summary, sintering is mainly responsible for the structural evolution because it is a process of densification driven by the tendency for reducing the internal energy [34]. The decrease in pore volume is consistent with the theories of sintering since sintering results in collapse of pores and decrease in porosity. Since the pore structure deteriorates at 800°C, it is clear that further study is required to improve the thermal stability of the composite membranes. It is noted that the unsupported membranes available in this paper are designed for characterization, but the real membranes for application should be supported by porous materials to obtain mechanical stability.

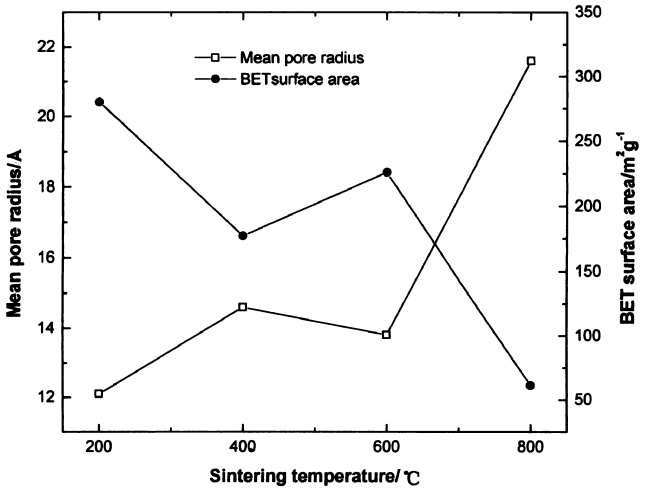

Fig. 10. Sintering temperature dependence of mean pore radius and BET surface area for composite membranes with 40 mol% SiO_2 content.

4. Conclusion

Unsupported Al_2O_3–SiO_2 composite membranes are prepared by the sol–gel method. XRD shows that when sintering from 200 to 1100°C, the membrane with 40 mol% SiO_2 goes through the following phase transformation: amorphous phase (200–800°C)→amorphous phase and crystalline γ-Al_2O_3 (1000°C)→mullite and α-Al_2O_3 (1100°C). Nitrogen adsorption measurements reveal that, in comparison with the single Al_2O_3 membrane, the composite membranes consist of both micropores and mesopores sintering at 600°C. The modification of Al_2O_3 membranes by 50 mol% SiO_2 content induces a 1-nm pore diameter decrease and about 100 $m^2\ g^{-1}$ surface area increase, as well as only a negligible drop of 0.0164 $cm^3\ g^{-1}$ in pore volume. This is due to the pore formation mechanism controlled by both the packing of Al_2O_3 particles and interpenetration of SiO_2 clusters. Further sintering results in a decrease in both the total pore volume and the surface area, as well as an increase in mean pore size and finally the collapse of pores, attributable to phase transformation and densification driven by the tendency for reducing the internal energy. Further study is required to improve the thermal stability of the composite membrane.

Acknowledgements

This work was financially supported by the Ministry of Education, the People's Republic of China (No. 98053301).

References

[1] T. Matsufuji, N. Nishiyama, M. Matsukata, K. Ueyama, J. Membr. Sci. 178 (2000) 25.
[2] C.S. Chen, W. Liu, S. Xie, G.G. Zhang, H. Liu, G.Y. Meng, D.K. Peng, Adv. Mater. 12 (2000) 1132.
[3] A.B. Fuertes, J. Membr. Sci. 177 (2000) 9.
[4] S. Navpreet, C. Munir, J. Food Eng. 38 (1998) 57.
[5] A.K. Prabhu, S.T. Oyama, J. Membr. Sci. 176 (2000) 233.
[6] N. Tsuyoshi, F. Takao, S. Motoyuki, Water Sci. Technol. 35 (1997) 137.
[7] H. Ohashi, H. Ohya, M. Aihara, T. Takeuchi, Y. Negishi, J. Fan, S.I. Semenova, J. Membr. Sci. 166 (2000) 239.
[8] K. Kajihara, K. Nakanishi, J. Mater. Res. 16 (2001) 58.
[9] K. Kuraoka, Y. Chujo, T. Yazawa, J. Membr. Sci. 182 (2001) 139.
[10] Y.S. Lin, A.J. Burggraaf, J. Am. Ceram. Soc. 74 (1991) 219.
[11] A.F.M. Leenaars, K. Keizer, A.J. Burggraaf, J. Mater. Sci. 19 (1984) 1077.
[12] D.R. Pesiri, R.C. Snow, N. Elliott, C. Maggiore, R.C. Dye, J. Membr. Sci. 176 (2000) 209.
[13] P. Huang, N. Xu, J. Shi, J. Membr. Sci. 173 (2000) 159.
[14] G.Z. Cao, H.W. Brinkman, J. Meijerink, K.J. deVries, A.J. Burggraaf, J. Am. Ceram. Soc. 76 (1993) 2201.
[15] B.N. Nair, W.J. Elferink, K. Keizer, H. Verweij, J. Colloid. Interf. Sci. 178 (1996) 565.
[16] M. Natio, K. Nakahira, Y. Fukuda, H. Mori, J. Tsubaki, J. Membr. Sci. 129 (1997) 263.

[17] K.N.P. Kumar, K. Keizer, A.J. Burggraaf, T. Okubo, H. Nagamoto, J. Mater. Chem. 3 (1993) 923.
[18] P. Puhlfürß, A. Voigt, R. Weber, M. Morbé, J. Membr. Sci. 174 (2000) 123.
[19] R.J.R. Uhlhorn, V.T. Zaspalis, K. Kerzer, A.J. Burggraaf, J. Mater. Sci. 27 (1992) 538.
[20] J.R. Miller, W.J. Koros, Sep. Sci. Technol. 25 (1990) 1257.
[21] R.J.R. Uhlhorn, M.H.B.J. Huis, I. Veld, K. Keizer, A.J. Burggraaf, J. Mater. Sci. Lett. 8 (1989) 1135.
[22] G. Xomeritakis, Y.S. Lin, AIChE J. 44 (1998) 174.
[23] C.I. Lin, D.L. Flowers, J. Membr. Sci. 92 (1994) 45.
[24] J. Randon, R. Paterson, J. Membr. Sci. 134 (1997) 219.
[25] X.R. Huang, G.L. Meng, Z.T. Huang, J.M. Geng, J. Membr. Sci. 133 (1997) 145.
[26] B.N. Nair, T. Yamaguchi, T. Okubo, H. Suematsu, K. Keizer, S.I. Nakao, J. Membr. Sci. 135 (1997) 237.
[27] K.L. Yeung, J.M. Sebastian, A. Varma, J. Membr. Sci. 131 (1997) 9.
[28] I.H. Cho, S.B. Park, S.J. Cho, R. Ryoo, J. Catal. 173 (1998) 295.
[29] Chapter 7 C. Guizard, in: A.J. Burggraaf, L. Cot (Eds.), Fundamentals of Inorganic Membrane Science and Technology, Elsevier, Amsterdam, 1996, p. 227.
[30] K. Kaneko, J. Membr. Sci. 96 (1994) 59.
[31] Q. Xu, M.A. Anderson, J. Am. Ceram. Soc. 77 (1994) 1939.
[32] A.F.M. Leenaars, K. Keier, A.J. Burggraaf, J. Colloid. Interf. Sci. 105 (1985) 27.
[33] D.L. Logan, C.S. Ashley, C.J. Brinker, Mater. Res. Soc. Symp. Proc. 271 (1992) 541.
[34] J. Kim, Y.S. Lin, J. Membr. Sci. 139 (1998) 75.